17

# Performance Optimization in Machining of Aluminium Alloys for Moulds Production: HSM and EDM

Andrea Gatto[1], Elena Bassoli[1] and Luca Iuliano[2]
[1]*University of Modena and Reggio Emilia*
[2]*Politecnico di Torino*
*Italy*

## 1. Introduction

In order to face the demands of today's competition, i.e. short time-to-market for customized products in small batches, in the field of moulds construction a growing interest is seen for materials that combine high mechanical properties with the possibility of a quicker and easier machining (Klocke, 1998). Aluminium alloys offer many machining advantages such as excellent machinability and finish degree with high cutting speed, low cutting forces, outstanding tool life (Kishawy et al., 2005; Schultz & Moriwaki, 1992). Elevated thermal exchange and weight reduction, which means easier handling, compared to steels are additional characteristics that lead to increasing applications in the automotive and aerospace industry and in the field of mould production (Amorim & Weingaertner, 2002; Ozcelik et al., 2010). The use of Aluminium moulds, whose thermal conductivity is up to 5 times higher than of traditional steel moulds, ensures an impressive reduction of cooling time at closed mould, which is the longest step in polymers injection moulding cycle. Moreover, high thermal exchange promotes a better workpiece accuracy, lower risk of warpage and sink marks, lower molded-in stresses (Erstling, 1998). Good corrosion resistance of Aluminium is an additional advantage in processing molten polymers. Relatively recent Aluminium alloys derived by aeronautical uses offer high tensile strength and hardness: the gap with steels is thus reduced or even reversed in terms of specific properties (Amorim & Weingaertner, 2002; Starke & Staley, 1996). Wrought heat-treatable alloys develop high specific strength thanks to age-hardening and have been widely used for airframes. Above all Al-Cu alloys (2xxx series) and Al-Zn alloys (7xxx series) are recognized for best damage tolerance and strength, respectively (Starke & Staley, 1996). The addition of transition elements, i.e. Cr, Mn or Zr, leads to dispersions capable of controlling the grain structure. Two examples of such alloys are Al 2219 and Al 7050, which are good candidates for injection moulds applications.
If the first examples of Aluminium moulds for plastic injection were limited to preproduction, the properties of these new alloys match the requirements of medium production volumes (up to 10000 parts/ year), which today are also the main market demand (Miller & Guha, 1998; Erstling, 1998; Klocke, 1998; Amorim & Weingaertner, 2002; Pecas et al., 2009).

Two machining operations are typically required in the tooling phase: milling, to produce the overall mould cavity and functional features, and Electro Discharge Machining (EDM), to obtain specific surface textures or complex geometrical details (Klocke, 1998; Lopez De Lacalle et al., 2002).

As to milling operation, several studies prove that Aluminium alloys allow the advantageous adoption of high cutting speed, in the field of High Speed Machining (HSM), which ensures time and cost savings together with excellent surface finish and dimensional accuracy with low tool wear and reduced bur formation (Chamberlain, 1979; Schultz & Moriwaki, 1992). In the case of Aluminium alloys, cutting speed can be increased up to one order of magnitude above the current practice, leading to important industrial profits.

Due to the combination of increased productivity and high quality, HSM has obviously become one of the most promising manufacturing technologies in recent decades, and has been applied in a lot of fields, such as aeronautics and astronautics, automobile, die, and mould industries (Bassoli et al., 2010; Kishawy et al., 2005). Besides the above improvements, HSM can even broaden the production capabilities foe example of thin webs, since it involves peculiar cutting conditions, characterized by low cutting forces and low surface temperatures (Kishawy et al., 2005). At high cutting speed, feed and depth of cut can be reduced without cutbacks on material removal rate or machining time: cutting stress is thus decreased. Moreover, high-speed cutting of Al alloys has almost no detrimental effect on tool wear. Even if high chip temperature is obtained, even near to the melting point, this is not enough to activate diffusion wear on most of today's tool materials. Hence only mechanically-activated wear mechanisms occur, in the form of flank wear (Kishawy et al., 2005; Yoshikawa & Nishiyawa, 1999). Schultz and Moriwaky (1992) outline that the material-specific cutting mechanisms in HSM influence the whole cutting process, including cutting parameters as well as tool, machine components and strategies. Many authors agree that the high-speed field is difficult to be defined and is relative to the work piece material. Some researchers believe that HSM can be identified as the domain where shear-localization develops almost completely in the primary shear zone (Kishawy et al., 2005), but for others this phenomenon can be ascribed only to hard alloys giving segmental chip. High thermal conductivity and low hardness of Aluminium alloys are responsible for continuous chip formation even under high speed cutting, unless the alloy is in the overaged state (Schultz & Moriwaki, 1992). Anyway, a limited secondary shear zone is certainly characteristic of high speed cutting.

For Aluminium alloys, values of cutting speed that are considered typical of HSM are in the range 1000 to 10000m/ min, but optimum results were obtained for 3500-4500m/ min with feed rates between 5000 and 10000mm/ min (Schultz, 1984). Lower surface roughness can be obtained than for conventional machining. Despite the described potential, many issues still need to be addressed before the full industrial exploitation of HSM. Traditional laws between cutting parameters do not apply to the field of high-speed machining and the mechanisms of chip removal still need investigation (Kishawy et al., 2005).

EDM is used for the machining of complex shapes and textures typical of plastic injection moulds. EDM is one of the most widespread non-conventional material removal processes (Ho & Newman, 2003). The material removal mechanism is based on spark erosion: electrical energy is turned into thermal energy through a series of discrete electrical discharges occurring between the electrode and workpiece immersed in a dielectric fluid (Tsai et al., 2003). A plasma channel is generated between cathode and anode (Shobert, 1983) at a temperature in the range of 8000 to 12000°C (Diver et al., 2004) or as high as 20000°C (Pham et al 2004). A volume at the surface of each pole is heated and molten. When the

pulsating direct current supply, occurring at the rate of approximately 20000–30000Hz (Liu et al., 2005), is turned off, the plasma channel breaks down. The temperature suddenly drops and the plasma channel implodes due to the circulating dielectric: the molten material is flushed from the pole surfaces in the form of microscopic debris (Ho and Newman, 2003). The described mechanisms produces a variety of micro-features on the EDMed surface. In addition to overlapping craters and resolidified material, in the form of globules or splashes, cracks and a thermally affected layer can be present (Lee & Tai, 2003). The heat-affected layer is quite different from the original material and, although it can be beneficial in terms of enhanced abrasion and erosion resistance, it introduces a variation in the mechanical properties that should be carefully controlled. The process does not involve any contact between the tool and the workpiece. Thereby, machining forces are negligible and electrically conductive materials can be machined regardless of their strength and hardness (Lee & Tai, 2003; Kuppan et al., 2008; Tan and Yeo, 2008). Distinctive advantages can be obtained in the production of complex geometrical features and small details, i.e. in the manufacture of moulds, dies, automotive, aerospace and surgical components. In die-sinking EDM the electrode feeds into the workpiece removing material by spark erosion until its geometry is mirrored in the part (Simao et al., 2003; Guu et al., 2003). The main process parameters are peak current during current supply, its duration or pulse-on-time and the delay interval before next peak, or pulse-off-time, and the average voltage between electrode and workpiece through the gap. Pulse power and energy are detemnined by the pulse intensity and duration, while the flushing and cooling efficacy depend on the duty factor, ratio between the pulse-on-time and the overall cycle duration. Machining accuracy depends on the electrode tolerances, on the gap between the electrode and the workpiece, which varies with the machining parameters and the local geometry, and on wear. In particular, wear of the electrode along the feed direction can be compensated, but wear along the cross-section turns into part inaccuracy (Khan, 2008). EDM is a complex process influenced by a number of variables and subject to many error sources. Thermal, chemical and electrical phenomena interact in the sparking process, which has a stochastic nature (Pham et al 2004). The occurrence of discharges is a probabilistic phenomenon whose distribution is not random but chaotic, which means that even if the system develops in every moment following deterministic rules, the final outcome can not be predicted and its time evolution appears random, because the initial condition of the system affects the subsequent events dramatically (Han and Kunieda, 2001). Hence, modelling and predicting the process performances is a challenging problem and process set-up is often based on experimental data (Pham et al 2004).

As regards EDM of Aluminium alloys, literature studies concerning the machining performances are quite rare. Amorim and Weingaertner (2002) identify process parameters for highest material removal rate, finding that duty factor higher than 0,8 promotes instability with short-circuit pulses. Khan (2008) evaluates electrode wear in EDMing of Aluminium and mild steel. It is claimed that higher thermal conductivity of Aluminium leads to comparatively higher energy dissipation into the workpiece than in the electrode, which turns into lower tool wear. As to the EDMed surface morphology, Miller and Guha (1998) report that the heat affected layer in Aluminium alloys is not harder than the base material and is not susceptible to cracking, unlike what is observed for steel. Some researchers dealt with surface modification through EDM, using specific electrodes and fluids to obtain hard layers with increased wear- and corrosion resistance (Lin et al., 2001; Mohri et al., 2008). Much is still to be studied as to machining accuracy and its link to electrode wear and EDMed surface morphology.

Aim of this research is to verify the HS- and ED Machinability of three Aluminium alloys: Al2219 and Al7050, derived from aeronautical applications, in addition to Al7075, which is more common for pre-series moulds, to provide control data. For both technologies the machining performance is evaluated in specific tests through a multiscale approach: measurements of the macroscopic process outputs are merged with the investigation of mechanisms at a microscopic level. The methodology enhances optimization chances with respect to traditional practice.

## 2. Materials and methods

The three alloys Al2219 (Al-Cu), Al7050 and Al7075 (Al-Zn) are provided as laminated and T6 heat treated. Composition, physical and mechanical characteristics of the three alloys are shown in Table 1.

| | | **Al2219 – T6** | **Al7050 – T6** | **Al7075 – T6** |
|---|---|---|---|---|
| Chemical composition (wt. %) | Cu | 6.345 | 1.804 | 1.528 |
| | Mn | 0.279 | 0.004 | 0.078 |
| | Zr | 0.1211 | 0.115 | 0.008 |
| | Fe | 0.111 | 0.080 | 0.290 |
| | Si | 0.053 | 0.040 | 0.159 |
| | Ti | 0.038 | 0.029 | 0.029 |
| | Zn | 0.028 | 6.260 | 5.800 |
| | Mo | 0.01 | 2.296 | 2.635 |
| | Pb | 0.008 | 0.003 | 0.003 |
| | Ni | 0.005 | 0.008 | 0.005 |
| | Cr | 0.001 | 0.003 | 0.192 |
| | Al | bal. | bal. | bal. |
| Brinell Hardness | | 115 | 147 | 150 |
| Young Modulus [GPa] | | 72 | 72 | 72 |
| Ultimate Tensile Strength [MPa] | | 452 | 579 | 432 |
| Yield stress [MPa] | | 348 | 515 | 316 |
| Elongation at break [%] | | 7.60 | 7.60 | 9.80 |
| Thermal conductivity [W/ mK] | | 120 | 153 | 130 |
| Melting Temperature [°C] | | 543 | 524 | 532 |

Table 1. Composition, physical and mechanical characteristics of the studied alloys

### 2.1 HSM tests

High speed face milling tests are performed using a 100mm diameter mill with 7 uncoated carbide inserts (ISO grade K) having a rake angle of 30°. Inserts' geometry is shown in Figure 1. Cutting speed ($V$) is ranged from 600 to 2200m/ min and feed per tooth ($f_z$) between 0.075 and 0.18mm/ tooth·rev, corresponding to values of table speed between 1000 and 7000mm/ min. A full $4^2$ factorial plan is adopted, with the levels in geometric progression as shown in Table 2. The tests are performed across the lowest limit of HSM, to investigate the variations in chip formation mechanisms when the high speed cutting regime is initiated. Axial depth of cut is kept constant at 2mm. The operations are performed

on a CNC milling machine with 3 controlled axes with maximum spindle speed of 8000rpm. Preliminary tests proved that the set of parameters V=220m/ min; $f_Z$=0.18mm/ tooth·rev exceeds the maximum machine power. For this specific test feed per tooth is thus reduced to 0.14mm/ tooth·rev. Each test was stopped after a machined volume of 150cm$^3$.

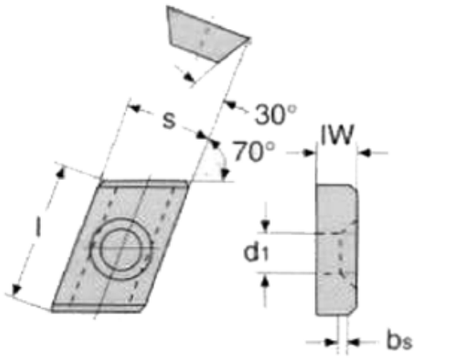


| Dimensions [mm] | | | | |
|---|---|---|---|---|
| l | s | $d_1$ | IW | $b_s$ |
| 12,77 | 10,0 | 4,1 | 3,5 | 0,9 |

Fig. 1. Geometry of the inserts

| | |
|---|---|
| V [m/ min] | 600 – 925 – 1426 - 2200 |
| $f_z$ [mm/ tooth·rev] | 0.075 – 0.1 – 0.13 - 0.18 |

Table 2. Levels of cutting speed and feed per tooth used in the HSM tests

The effect of cutting parameters on surface roughness, tool wear and chip formation mechanisms are studied with the aid of SEM observation and EDX semi-quantitative analysis, as well as through multiple regression analysis.

Average roughness ($R_a$) is measured on the milled surfaces with a stylus meter (Hommel T1000), using a sampling length of 15 mm. Five measurements are performed on each specimen. Tool inserts are observed through optical- and scanning electron microscope (OM, SEM) to evaluate wear mechanisms and entity. On chip produced during the milling tests a wider and more complex analysis is carried out. Chip dimensions and morphology are analyzed through OM, then SEM observation is adopted on both convex and concave chip surfaces to investigate tool-chip interaction and chip formation mechanisms. Moreover, chip samples are embedded in epoxy resin and sectioned perpendicularly to the cutting edge. The sections are polished through SiC papers and diamond sprays up to 1μm. Etching is carried out to study grain shape and dimensions, as well as deformation. Keller's reagent is used (Table 3) for 5÷30 s.

| | |
|---|---|
| **HF (48% soln.)** | 1 |
| **HCl (conc.)** | 1.5 |
| **$HNO_3$ (conc.)** | 2.5 |
| **$H_2O$** | 95 |

Table 3. Composition of Keller's reagent (vol. %)

### 2.2 EDM tests

As to EDM, in addition to surface roughness and erosion mechanisms, dimensional accuracy is also addressed. Hence a specific benchmark geometry is defined for the electrode, shown in Figure 2. It allows pointing out the typical problems of moulds machining: different geometrical features are present to outline dimensional accuracy, eroded surface morphology and electrode wear both parallel and orthogonal to the feed direction, as well as on concave and convex edges.

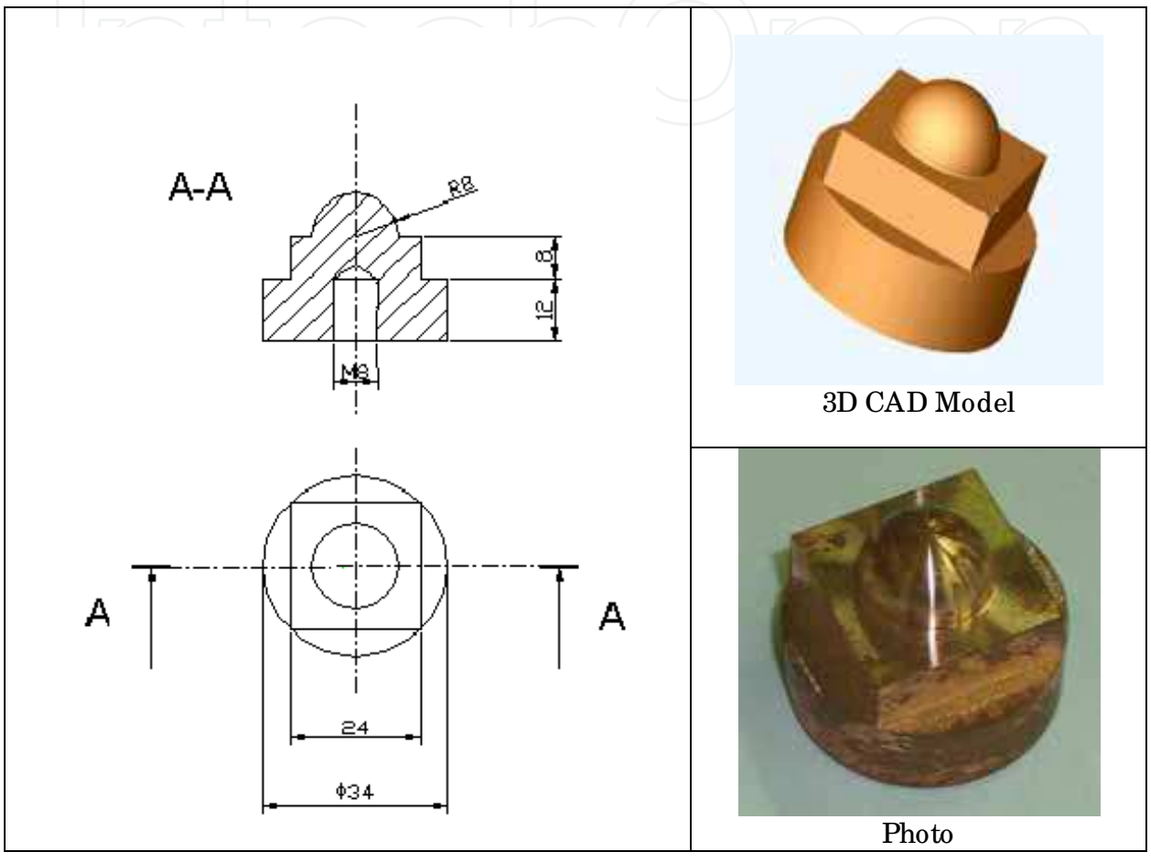


Fig. 2. Geometry of the electrodes employed in the tests

Electrolytic copper electrodes are produced and used to machine the three Aluminium alloys through three steps: roughing, semifinishing and finishing. Process parameters suggested by the machine producer are adopted in each phase, as listed in Table 4. It is important to notice that these parameters refer generically to Aluminium to be processed with Copper electrodes, whereas no specification is available for the single alloy. Machining is performed with a vertical movement in the Z direction of the electrode holder. Roughing operations are performed leaving 2mm stock, reduced to 0.5 mm after the semifinishing step. The total machined depth of the finished specimens is 20mm.

A commercial dielectric fluid specific for EDM is adopted (ELECTROFLUX DF – ATIUR). Every test is repeated three times, with the same procedure and process parameters on each alloy. Figure 3 shows a machining step.

Specimens are obtained separately for the three machining steps: after roughing, after roughing and semifinishing, and after the complete cycle up to finishing. A new electrode is employed to produce each sample.

| | Roughing | Semifinishing | Finishing |
|---|---|---|---|
| **Supply voltage [V]** | 31 | 48 | not specified |
| **Peak current [A]** | 35 | 25 | 7,3 |
| **Gap [mm]** | 0,250-0,375 | 0,135-0,210 | 0,020-0,043 |
| **Electrode polarity** | + | + | + |

Table 4. EDM parameters used in the tests

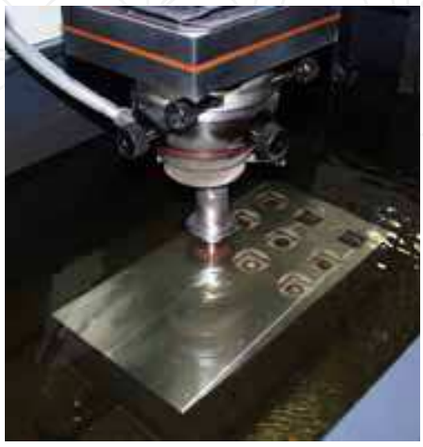

Fig. 3. Machining phase

For each specimen, the following measurements are carried out:
- dimensional measurements on the electrodes in order to study wear in relation to the type of operation and alloy;
- dimensional measurements on the workpieces, to evaluate machining tolerance relative to the type of operation and alloy;
- roughness measurements on the workpieces.

Dimensional measurements are performed with a coordinate measuring machine (CMM), evaluating the geometrical features shown in Figure 4. Roughness measurements are obtained with a contact stylus meter with a sampling length of 4.8mm.

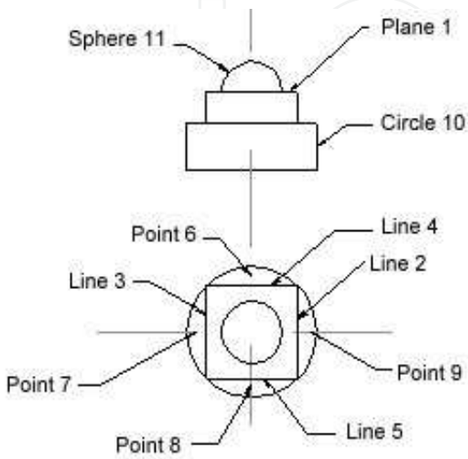


Fig. 4. Geometrical elements measured on workpieces and electrodes

Both the electrodes and the workpieces are sectioned by micro-cutting: a cut containing the benchmark axis is obtained and 5mm thick slices are then produced (Figure 5). Axial sections are polished up to 1μm diamond paste and chemical etched, using potassium dichromate on copper and fluoro-hydrochloric reactant on the Al alloys. OM observation is performed to evaluate wear entity and shape accuracy, taking into account also eventual variations for the different local geometry and orientation. The presence of outer heat-affected or molten and re-solidified layer is also investigated.

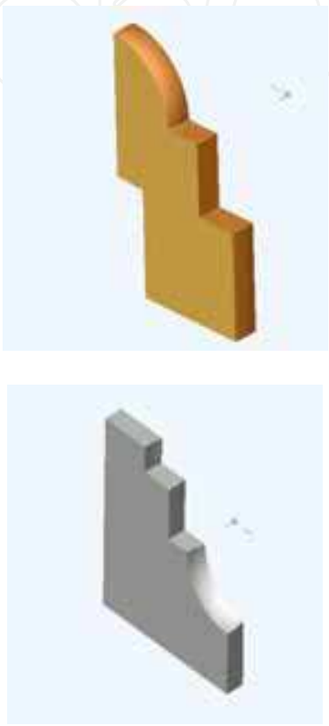

Fig. 5. Electrode and workpiece sections (5 mm)

SEM observation is carried out to verify the presence and composition of deposits on the worn electrode surfaces, as well as the eroded surfaces morphology on the workpieces.

## 3. Results and discussion

### 3.1 HSM tests

All the inserts show uniform wear: notches, breaks or craters are not observed. For each parameter combination flank wear ($V_B$) is measured through OM and surface roughness ($R_a$) by the stylus meter; all the results are summarized in Table 5. $V_B$ and $R_a$ are analyzed through statistical tools. Multiple regression models are evaluated including as independent variables: feed per tooth and cutting speed, their product and their squares. The significance of models and of regression parameters is checked by variance analysis.

***Tool wear***

Tool wear is very low for all the tests, observation of the inserts prove that abrasive effects causing the backward motion of the cutting edge are minimal. The volume machined for every test is very far from the tool life limit.

| | | Al 7075 | | Al 7050 | | Al 2219 | |
|---|---|---|---|---|---|---|---|
| V [m/min] | $f_Z$ [mm/tooth rev] | $V_B$ [mm] | $R_a$ [µm] | $V_B$ [mm] | $R_a$ [µm] | $V_B$ [mm] | $R_a$ [µm] |
| 600 | 0.075 | 0.12 | 0.39 | 0.14 | 0.16 | 0.08 | 0.37 |
| 600 | 0.100 | 0.13 | 0.41 | 0.27 | 0.28 | 0.11 | 0.41 |
| 600 | 0.130 | 0.14 | 0.45 | 0.25 | 0.39 | 0.12 | 0.41 |
| 600 | 0.180 | 0.21 | 1.90 | 0.30 | 0.53 | 0.14 | 0.63 |
| 925 | 0.075 | 0.10 | 0.31 | 0.19 | 0.21 | 0.09 | 0.36 |
| 925 | 0.100 | 0.11 | 0.32 | 0.22 | 0.18 | 0.11 | 0.50 |
| 925 | 0.130 | 0.17 | 0.53 | 0.22 | 0.74 | 0.11 | 0.25 |
| 925 | 0.180 | 0.21 | 1.07 | 0.31 | 1.06 | 0.12 | 0.73 |
| 1426 | 0.075 | 0.10 | 0.17 | 0.17 | 0.15 | 0.14 | 0.40 |
| 1426 | 0.100 | 0.15 | 0.33 | 0.20 | 0.20 | 0.14 | 0.31 |
| 1426 | 0.130 | 0.18 | 0.39 | 0.21 | 0.34 | 0.17 | 0.44 |
| 1426 | 0.180 | 0.17 | 0.88 | 0.26 | 0.36 | 0.14 | 1.08 |
| 2199 | 0.075 | 0.15 | 0.23 | 0.15 | 0.10 | 0.16 | 0.24 |
| 2199 | 0.100 | 0.13 | 0.27 | 0.18 | 0.23 | 0.21 | 0.43 |
| 2199 | 0.130 | 0.12 | 0.44 | 0.20 | 0.29 | 0.19 | 0.69 |
| 2199 | 0.140* | 0.16 | 0.40 | 0.21 | 0.21 | 0.19 | 0.44 |

* Due to maximum power limits of the CNC machine

Table 5. Results for flank wear and surface roughness for the three alloys

Figures 6, 7 and 8 show plots of the regression models developed for the three alloys within the experimental domain. Experimental figures are superimposed as asterisks to the contour lines.

For the alloy 7075 the main affecting factors are cutting speed and feed per tooth according to the model described in equation (1), for which $R^2_{adj} = 0.70$.

$$V_B = -0.016 + 0.000065\,V + 1.4\,f_Z - 0.00058\,V \cdot f_Z \quad (1)$$

If the plot in Figure 6 is observed, it can be remarked that wear is minimum for low values of cutting speed and feed per tooth; it increases for high values of feed per tooth in the field of low cutting speed or for high values of cutting speed if feed per tooth is quite low. Amongst the last two unfavourable cases, the first condition (low cutting speed and high feed per tooth) gives the worst results and should be carefully avoided for this alloy.

Further considerations can be made by dividing the diagram into three areas:

- middle values of feed per tooth: wear is almost unaffected by increasing cutting speed;
- high values of feed per tooth: wear decreases when cutting speed increases;
- low values of feed per tooth: wear increases with cutting speed.

For alloy 7050 the best fit of experimental data is obtained with the model in equation (2), which involves only feed per tooth and the product of feed per tooth and cutting speed. The model describes a big fraction of the total variance ($R^2_{adj} = 0.81$).

$$V_B = 0.1016 + 1.35\,f_Z - 0.00031\,V \cdot f_Z \quad (2)$$

Figure 7 outlines that the highest tool wear is obtained for high values of feed per tooth, in the same area as observed for alloy 7075. By increasing cutting speed, tool wear improves at any value of feed per tooth: the best result is obtained with high values of cutting speed and low values of feed per tooth.

For alloy 2219, the model includes not only cutting speed, feed per tooth and their product, but also square feed per tooth. The model, described by equation (3), provides a very good fit of experimental data ($R^2_{adj} = 0.86$).

$$V_B = -0.086 + 0.00004\,V + 2.46\,f_Z - 7.43^*\,f_Z^2 - 0.00023\,V\cdot f_Z \quad (3)$$

It is evident in Figure 8 that highest wear is produced by intermediate values of feed per tooth and middle-high cutting speed. In the area of high cutting speed, both low and high values of feed per tooth yield to similar limited wear.

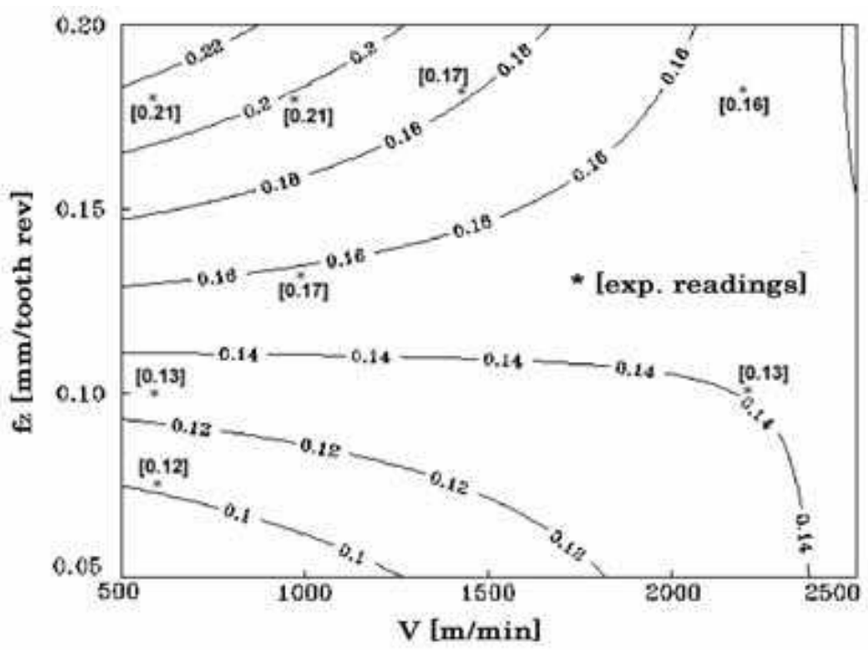


Fig. 6. Flank wear $V_B$ [mm] versus cutting speed and feed per tooth for the alloy 7075

***Surface roughness and chip formation mechanisms***

Surface finish is generally very good for all the tests. Multiple regression analysis on the measurements of surface roughness leads to models that are not completely satisfactory for any of the three alloys, hence they are not proposed. Figure 9 shows a scatterplot of surface roughness values in the experimental domain, where the results for the three alloys can be compared. It can be observed that for all the alloys surface roughness shows strong increases with increasing feed per tooth in the range of low-medium cutting speed. If high cutting speed is adopted, instead, smoother surfaces are obtained even for high values of feed. Better results are in general obtained for alloy 7050 than for 7075, in particular as to the maximum values. The observed trend suggests that the mechanisms of chip removal are positively affected by the use of high cutting speed in the considered experimental domain, with some disparities even for alloys that are very similar in composition. These aspects are further studied though the observation of chip morphology.

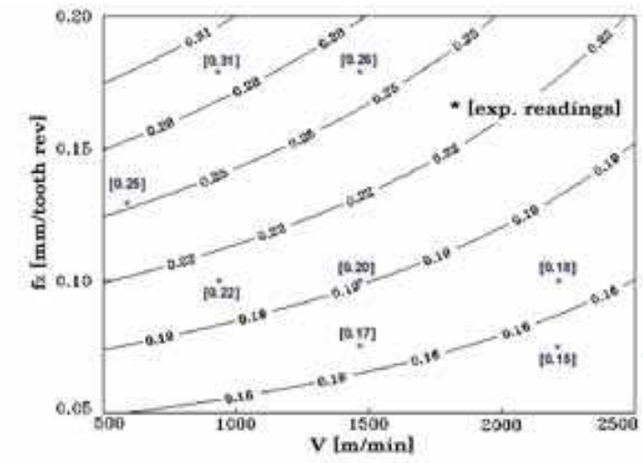


Fig. 7. Flank wear $V_B$ [mm] versus cutting speed and feed per tooth for the alloy 7050

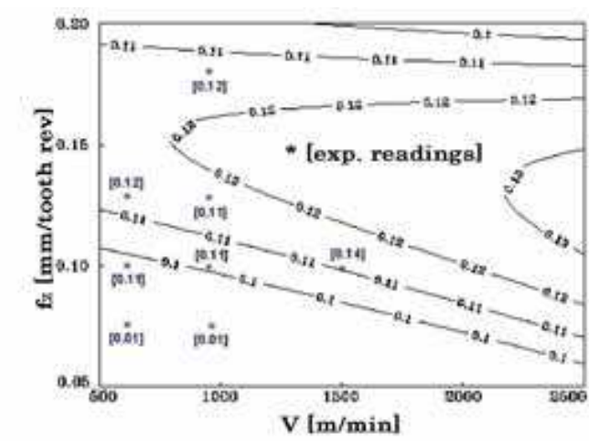


Fig. 8. Flank wear $V_B$ [mm] versus cutting speed and feed per tooth for the alloy 2219

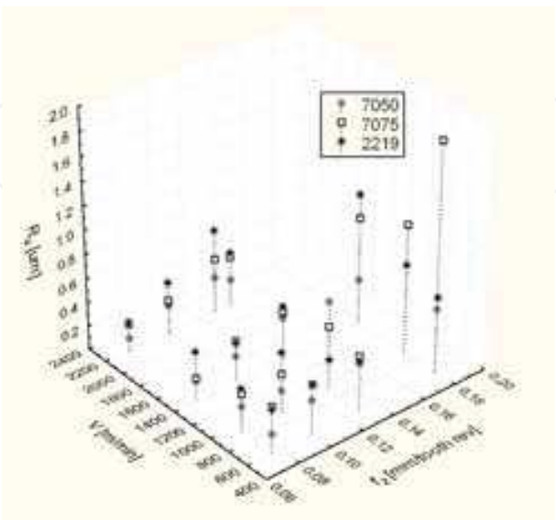


Fig. 9. Scatterplot of $R_a$ versus cutting speed and feed per tooth for the three alloys

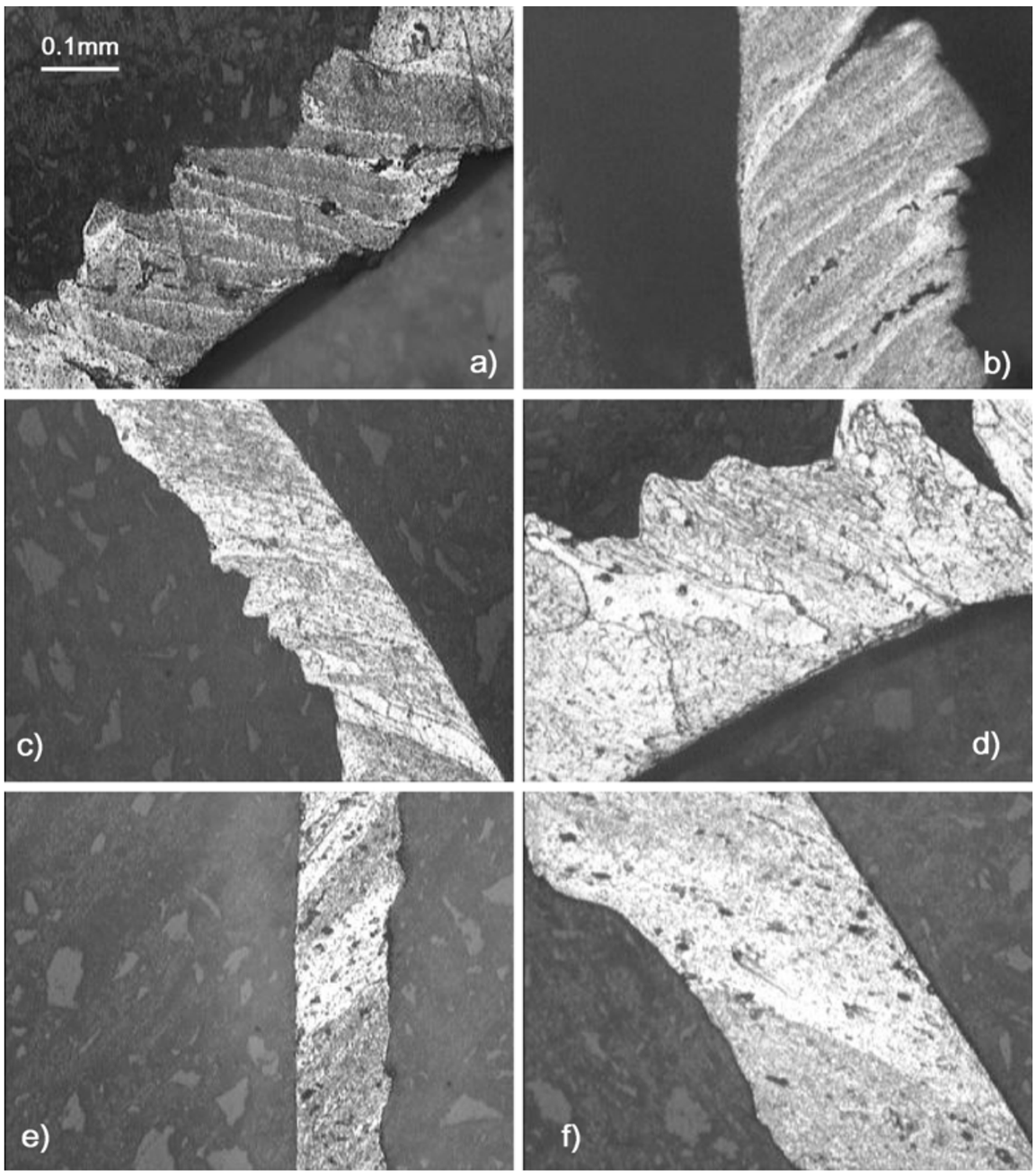


Fig. 10. Optical micrographies of chip sections after etching corresponding to the minimum (a,c,e) and maximum (b,d,f) roughness of the machined surface. Alloy 7075: a) V=1426m/ min, $f_Z$=0.075 mm/ tooth·rev and b) V=600m/ min, $f_Z$=0.18mm/ tooth·rev. Alloy 7050: c) V=2199m/ min, $f_Z$=0.075 mm/ tooth·rev and d) V=925m/ min, $f_Z$=0.18mm/ tooth·rev. Alloy 2219: e) V=2199m/ min, $f_Z$=0.075 mm/ tooth·rev and f) V=1426m/ min, $f_Z$=0.18mm/ tooth·rev

Figure 10 shows longitudinal sections after chemical etching of chip corresponding to the minimum and maximum roughness value of the machined surface for the three alloys. Chip formation is well consistent with Pijspanen's model. Shear planes and non-homogeneous grain distribution can be observed. For Al 7050 and 7075 the secondary shear zone is evident only for low cutting speeds, whereas for alloy 2219 it occurs at any speed, even if it becomes less pronounced if cutting speed is high. This behaviour is consistent with HSM mechanisms reported in literature. Feed does not show a clear effect on secondary shear deformation.
Convex chip surface, i.e. the one interested by the contact with the tool face, is shown in Figure 11 for the three alloys. Chip are obtained with V=2199m/ min and $f_Z$=0.075 mm/ tooth·rev, which yield to roughness values that are minimum for two alloys and very near to the minimum for the other. The smoother surface is observed for Al 7050, free from micro-groves and tears that are present for alloy 2219 and, to a very high extent, for 7075. These observations account for a smoother tool-chip interaction, lower friction, lower adhesion and more regular mechanisms of chip formation for alloy 7050 in comparison to the others. Alloy 7075, in particular, provides the worst results. This outcome is consistent with the differences in surface roughness obtained on the workpieces. It is remarkable to conclude that the two alloys of the 7xxx series, even if very similar in composition and mechanical characteristics, provide significantly different results by HSM. Better surface finish of Al7050 could be ascribed to the higher weight percentage of Zr, that controls grains dimension and distribution.

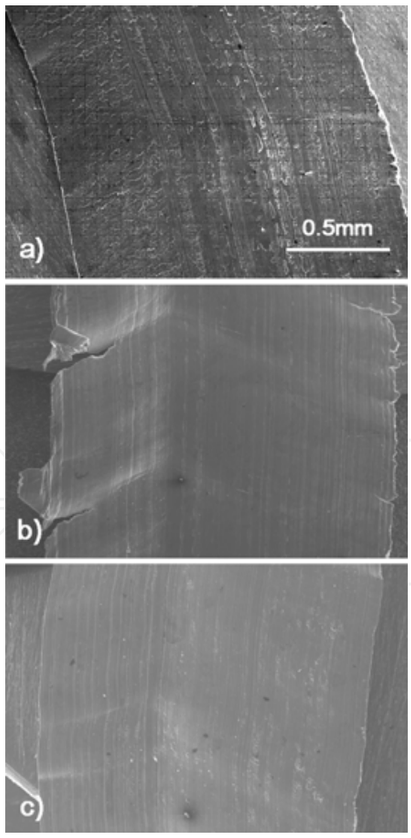


Fig. 11. SEM images of convex chip surface corresponding to V=2199m/ min, $f_Z$=0.075 mm/ tooth·rev: a) Al7075; b) Al7050; c) Al2219

### 3.2 EDM tests

***Dimensional accuracy***

Figure 12 shows some workpieces after the three steps of the EDMing cycle, ready for the CMM measurements.

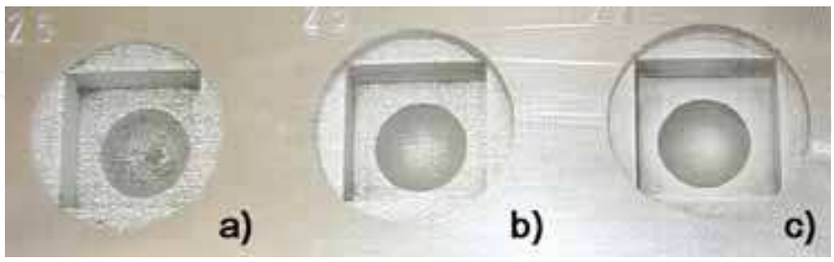


Fig. 12. Workpieces obtained after the operations of roughing (a), semifinishing (b), finishing (c)

All the geometric elements in Figure 4 are measured on the new electrode, on the worn one after operation and on the workpiece. Measurements are compared to the nominal values to obtain the dimensional deviation. An example of the measurements relative to the sphere diameter (nominal value=8mm) is shown in Table 6, referring to the semifinishing step on Al2219.

The percent dimensional deviation between the workpieces and the electrodes before machining is then calculated for each of the three alloys and three EDM steps. Since not all the distributions of percent deviations are Gaussian, averaging the obtained values is not acceptable to estimate the dimensional accuracy of each operation. Thus, the deviation range corresponding to the $95^{th}$ percentile of observed data is chosen to assess the process dimensional performances (Table 7). For alloys 2219 and 7050 the deviation percentage decreases when the peak current is reduced from roughing to finishing.

Percent deviations are also calculated between the dimensions of the new and worn electrodes, to estimate wear entity. The results are summarized in Figure 13.

| | New electrode before semifinishing | Worn electrode after semifinishing | Workpiece after semifinishing |
|---|---|---|---|
| Measured diameter of sphere 11 [mm] | 8.17 | 8.22 | 8.25 |
| Deviation from nominal value [mm] | -0.17 | -0.22 | -0.25 |

Table 6. Example of dimensional measurements after an EDM step

***Surface roughness and erosion mechanisms***

Table 8 shows the results for roughness measured with the portable stylus after the different operations. Obviously, for all the three alloys surface roughness decreases as current intensity is reduced from roughing to finishing. The erosion mechanisms and the consequent surface morphology are deepened though OM and SEM observation.

Figures 14 and 15 show OM images of workpieces' etched sections, after roughing and finishing, for the three alloys. For an easier interpretation of the results, the vertical direction

| Alloy | Operation | Estimated Deviation Range (95% of observ.) |
|---|---|---|
| 7075 | Roughing | 2,6 - 2,7 % |
| | Semifinishing | 1,1 - 1,2 % |
| | Finishing | 1,9 - 2,0 % |
| 7050 | Roughing | 2,3 - 2,4 % |
| | Semifinishing | 1,9 - 2,0 % |
| | Finishing | 1,8 - 1,9 % |
| 2219 | Roughing | 2,4 - 2,5 % |
| | Semifinishing | 2,1 - 2,2 % |
| | Finishing | 1,9 - 2,0% |

Table 7. Percent dimensional deviation ranges calculated for the EDM operations

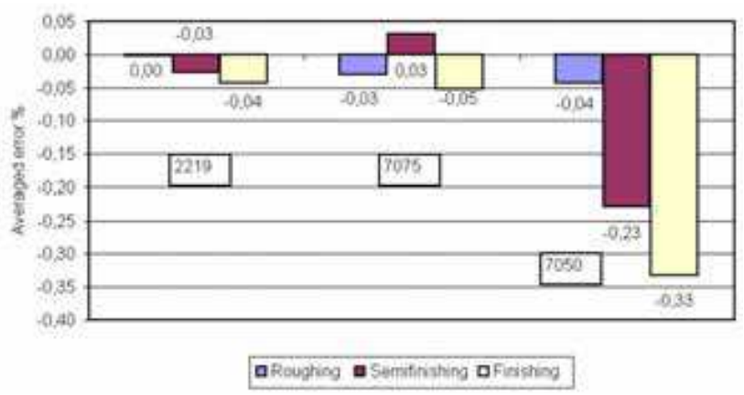


Fig. 13. Diagram of the dimensional deviation between new and worn electrodes

| Alloy | Operation | Ra [µm] |
|---|---|---|
| 7075 | Roughing | 9.0 |
| | Semifinishing | 4.5 |
| | Finishing | 1.1 |
| 7050 | Roughing | 12.5 |
| | Semifinishing | 4.5 |
| | Finishing | 1.6 |
| 2219 | Roughing | 9.0 |
| | Semifinishing | 6.3 |
| | Finishing | 2.2 |

Table 8. Roughness measured on the EDMed surfaces

of all the images coincides with the feed direction during the operations. The images refer to the areas A on the top of sphere 11 and D on plane 1. The radius in the spherical A zone is big enough to exclude a significant effect on the gap geometry during the operations, with respect to the planar area D. The two areas can thus be considered geometrically equivalent, whereas they strongly differ as to the machining time, which is roughly two times higher in the A zone. No significant disparities can be appreciated in the morphology of the two

areas, proving that machining depth and progressive electrode wear does not affect the erosion mechanisms and the obtained surface, which depends for each alloy only on the process parameters.
If the three alloys are compared, different morphologies are observed, suggesting different erosion mechanisms. The entity of the superficial molten and resolidified layer and of the thermally affected zone below decreases from Al 2219 to Al 7050, with middle results for Al 7075.
Figure 16 shows, as an example, the etched sections of electrodes used for roughing and finishing operation on alloy 2219. Observations on the worn electrodes appear very similar for the three alloys: all the operations produce craters on the electrode surface. The roughing step also yields to a large amount of deposits.
In Figures 17 and 18 SEM observations of workpieces and electrodes after roughing are shown. The morphology of EDMed surfaces, with craters surrounded by molten and re-solidified material, appears more regular for alloy 7050 compared to Al 7075, Al 2219 shows an intermediate behavior. The alloy 7075 shows evident surface cracks, not present in Al 2219 and 7050, the latter being also more uniform, with less re-solidified material.

## 7. Conclusion

The performance of HSM and EDM on aeronautical Aluminium alloys 7050, 7075 and 2219 are studied, with the aim to provide technological know-how for moulds production. In both cases the machining performance is evaluated in specific tests through a multiscale approach: measurements of the macroscopic process outputs are merged with the investigation of mechanisms at a microscopic level. The methodology enhances optimization chances with respect to traditional practice.
As to HSM, tool wear and surface roughness are investigated versus cutting parameters. Chip formation is also deepened to support macroscopic results. The best surface finish is obtained for Al 7050 with high cutting speed and low feed. Minimal tool wear is observed in the considered conditions. Microscope observation of tools and chip proves that surface finish is ruled by tool-chip adhesion and that alloys having almost the same chemical composition can provide substantially different results due to grain dimension and distribution.
EDM performances are evaluated in terms of surface finish, dimensional and geometrical accuracy of the workpieces and wear mechanisms of the electrodes. Moreover, SEM observation is performed to investigate the presence and composition of deposits on the electrode surfaces, as well morphology of EDMed surfaces. The chosen benchmark allows to evaluate machining quality in various geometrical configurations, which can influence the erosive mechanisms and are representative of the industrial operative conditions. No remarkable differences can be identified as to dimensional tolerances between the three alloys: results are satisfactory for all of them. A slight trend to give lower roughness values can be noticed for the alloy 7050. The results are coherent with the regular morphology observed on the machined surfaces of this alloy. The observation of the erosion mechanisms allows to affirm that, for the same process parameters and very similar finishing results, the morphology of the machined surface can be considerably different, for example as to cracks density.
The above considerations, together with the higher mechanical properties of Al 7050 with respect to 2219 and 7075, suggest its profitable use for moulds production.

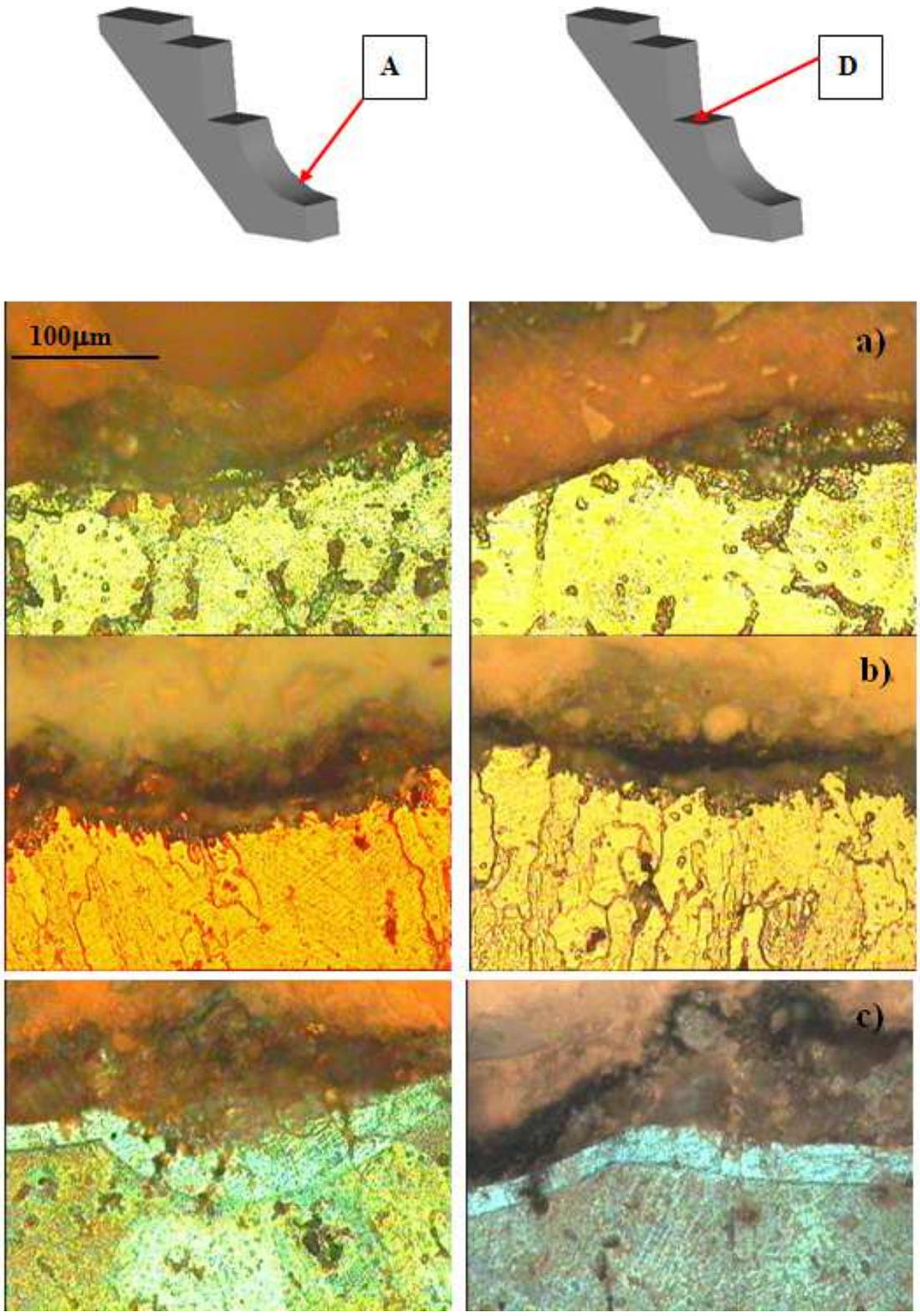


Fig. 14. Etched sections of roughed workpieces: a) Al 7075, b) Al 7050, c)Al 2219

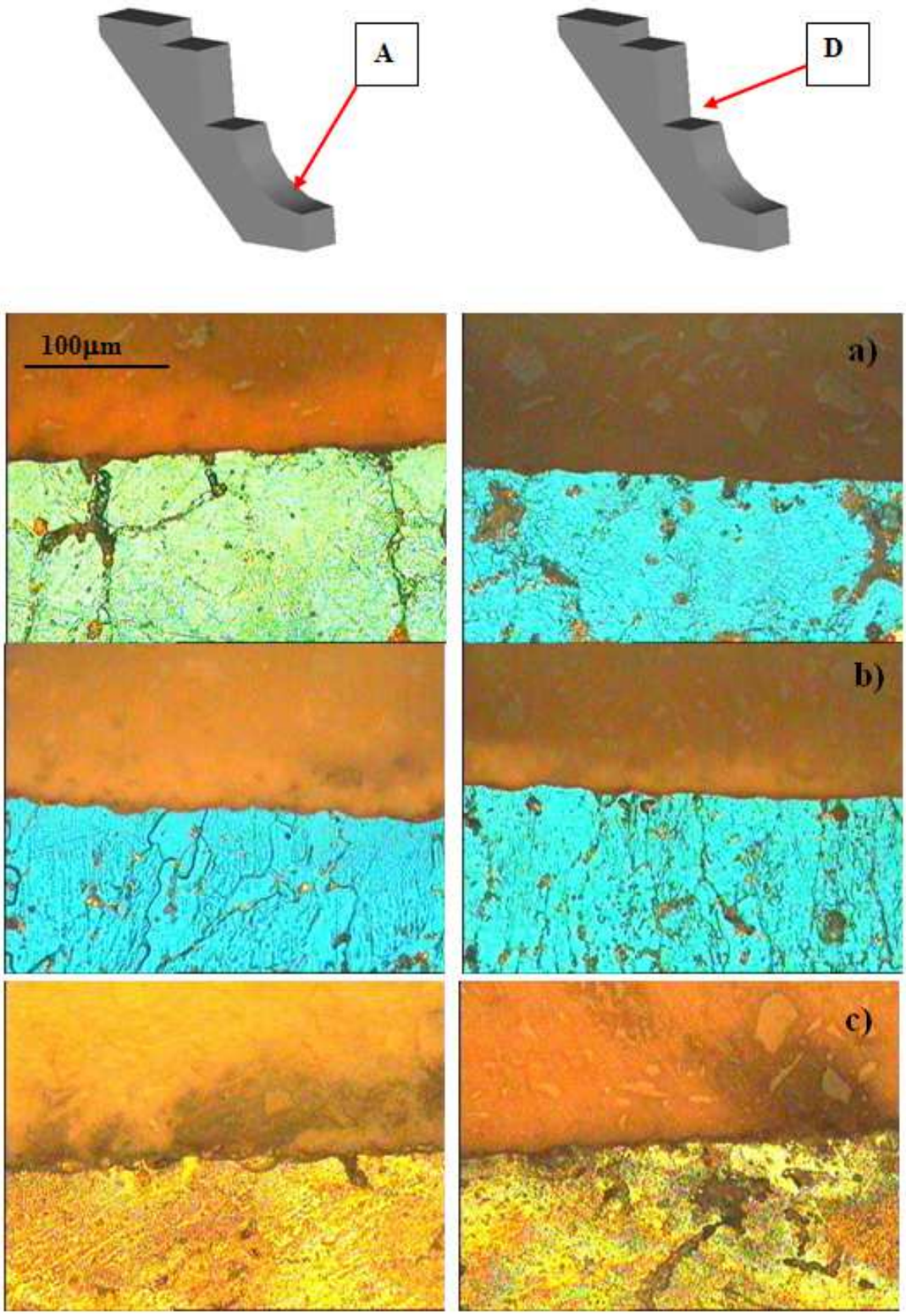


Fig. 15. Etched sections of finished workpieces: a) Al 7075, b) Al 7050, c)Al 2219

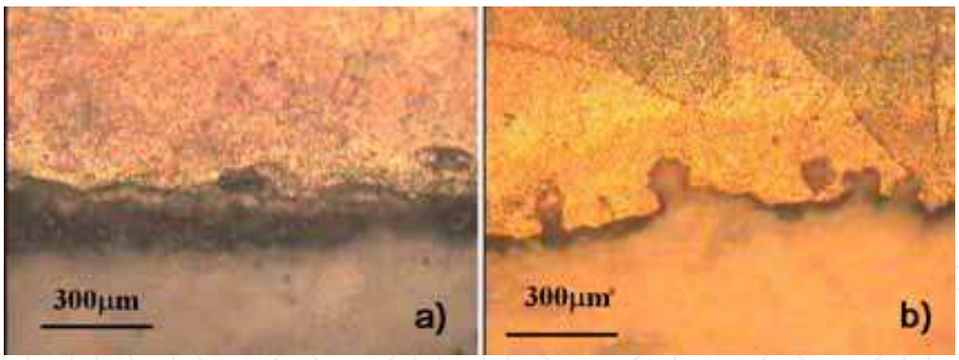


Fig. 16. Etched section of the electrode use for roughing (a) and finishing (b) on Al2219

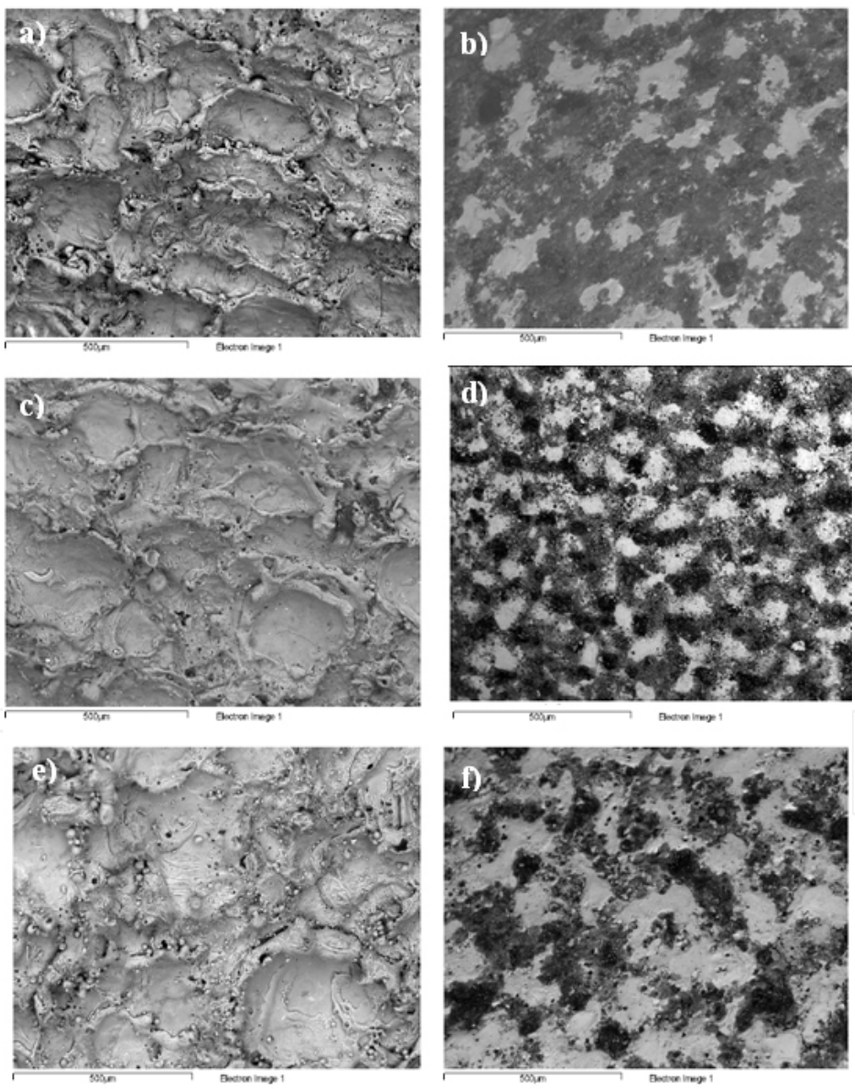


Fig. 17. Surfaces of the workpieces: a)Al 7075, c) Al7050, e)Al 2219 after roughing; and of the electrodes: b) Al 7075, d) Al7050, f)Al 2219; after roughing (A zone)

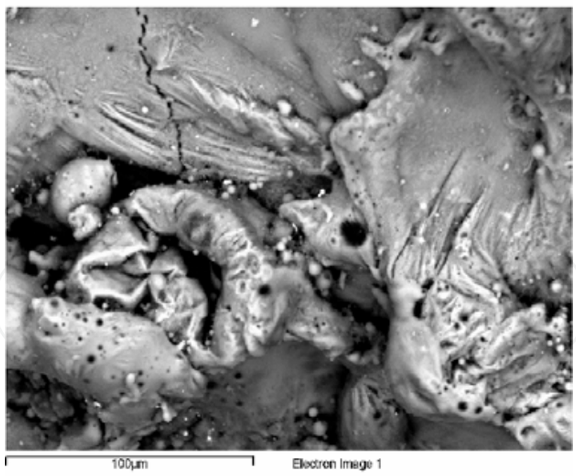


Fig. 18. Detail of Al7075 after roughing

## 8. References

Amorim, F.L. & Weingaertner, W.L. (2002). Influence of duty factor on the die-sinking Electrical Discharge Machining of high-strength aluminum alloy under rough machining, *J Braz. Soc. Mech. Sci.*, 24, 3, ISSN 0100-7386

Bassoli, E.; Iuliano, L. & Salmi, A. (2010). Deep drilling of Aluminium die-cast parts: surface roughness, dimensional tolerance, and tool-chip interaction, *Mat. and Manuf. Proc.*, 25, 6, 442 – 449, ISSN 1042-6914.

Chamberlain, B. (1979). Machinability of Aluminium Alloys, In: *Metals Handbook, Vol. 2—Properties and Selection: Nonferrous Alloys and Pure Metals - 9th Edition*, 187–190, ASM Intl., ISBN 0871700085.

Diver, C.; Atkinson, J; Helml, H.J. & Li, L. (2004). Micro-EDM drilling of tapered holes for industrial applications, *J Mater. Process. Technol.*, 149, 296–303

Erstling, A. (1998). Aluminium - Ein Werkstoff Inspiriert - Designer -Blasform, *Der Stahlformenbauer*,.6, 70-80.

Gatto, A. & Iuliano, L. (1994). Chip formation analysis in high speed machining of a nickel base superalloy with silicon carbide whisker-reinforced alumina, *Int. J Mach. Tool. Manu.*, 34, 8, 1147-1161, ISSN 0890-6955.

Gatto, A.; Iuliano, L. & Settineri, L. (1998). High-speed turning experiments on metal matrix composites, *Composites Part A*, 29, 12, 1501-1509, ISSN 1359-835X.

Gatto, A.; Iuliano, L.; Bassoli, E. & Violante, M.G. (2002). High speed milling of light alloys: tool performance and chip formation analysis, *Proceedings of ESDA 2002*, July 8-11 2002, Istanbul, Turkey.

Guu, Y.H.; Hocheng, H.; Chou, C.Y. & Deng, C.S. (2003). Effect of electrical discharge machining on surface characteristics and machining damage of AISI D2 tool steel, *Mat. Sci. and Eng. A*, 358, 1-2, 37-43

Han F., Kunieda, M. (2001). Chaos Found in Distribution of EDM Spark, *Proc. of ISEM XIII*, pp. 185–192.

Ho, K.H. & Newman, S.T., (2003). State of the art electrical discharge machining (EDM), *International Journal of Machine Tools and Manufacture*, 43,13, 1287-1300.

Iuliano, L.; Violante, M.G.; Gatto, A. & Bassoli, E. (2008). Study of the EDM process effects on Aluminum alloys, *Int. J Manufacturing Technology and Management, Special Issue on "Innovative approaches in Technology and Manufacturing Management"*, 14, 3-4, 326-341.

Khan, A.A. (2008). Electrode wear and material removal rate during EDM of aluminum and mild steel using copper and brass electrodes, *Int JAdv Manuf Technol,* 39, 482–487

Kishawy, H.A.; Dumitrescu, M.; Ng, E.-G. & Elbestawi, M.A. (2005). Effect of coolant strategy on tool performance, chip morphology and surface quality during high-speed machining of A356 aluminum alloy, *Int. J Mach. Tool. Manu.*, 45, 2, 219-227, ISSN 0890-6955

Klocke, F. (1998). The process sequence in tool and diemaking, *Proc. of the Int. Symposium for Electromachining*, pp. 65-97, Germany, May 11-13 1998, Vol. 1.

Kuppan, P.; Rajadurai, A. & Narayanan, S. (2008). Influence of EDM process parameters in deep hole drilling of Inconel 718, *Int JAdv Manuf Technol*, 38,74–84.

Lee, H.T. & Tai, T.Y. (2003). Relationship between EDM parameters and surface crack formation, *J Mater. Process. Technol.*, 142, 3, 676-683

Lin, Y.C.; Yan, B.H. & Huang, F.Y. (2001). Surface modification of Al-Zn-Mg aluminum alloy using the combined process of EDM with USM, *J Mater. Process. Technol.*, 115, 3, 359-366, ISSN 0924-0136

Liu, H.-S.; Yan, B.-H.; Huang, F.-Y. & Qiu, K.-H. (2005). A study on the characterization of high nickel alloy micro-holes using micro-EDM and their applications, *J Mater. Process. Technol.*, 169, 418–426

Lopez De Lacalle, L.N.; Lamikiz, A.; Salgado, M.A.; Herranz, S. & Rivero, A. (2002). Process planning for reliable high-speed machining of moulds, *Int. J of Production Res.*, 40, 12, 2789 – 2809.

Miller, P. & Guha, A. (1998). Effects of Electrical Discharge Machining on the surface characteristics of mold materials, The J. of injection molding technology, 2, 3, 128-135, ISSN 533-905X.

Mohri, N.; Saito, N.; Tsunekawa, Y. & Kinoshita, N. (1993) Metal Surface Modification by Electrical Discharge Machining with Composite Electrode, *CIRP Annals - Manufacturing Technology*, 42, 1, 219-222, ISSN 0007-8506.

Müller, C. & Blümke, R. (2001). Influence of heat treatment and cutting speed on chip segmentation of age hardenable aluminium alloy, *Mat. Sci. and Tech.*, 17, 6, 651-654.

Pecas, P.; Ribeiro, I.; Folgado, R. & Henriques, E. (2009). A Life Cycle Engineering model for technology selection: a case study on plastic injection moulds for low production volumes, *J of Cleaner Production*, 17, 9, 846-856, ISSN 0959-6526

Pham, D. T.; Ivanov, A.; Bigot, S.; Popov, K. & Dimov, S. (2007). An investigation of tube and rod electrode wear in micro EDM drilling, *Int JAdv. Manuf. Technol.*, 33, 103–109.

Ozcelik, B.; Ozbay, A. & Demirbas, E. (2010). Influence of injection parameters and mold materials on mechanical properties of ABS in plastic injection molding, *Int. Comm. in Heat and Mass Transfer*, In Press, ISSN 0735-1933

Schultz, H. (1984). High speed milling of aluminium alloys, High SpeedMachining, ASME, New York.

Schultz, H. & Moriwaki, T. (1992). High-speed machining. *Annals of the CIRP*, 41, 2, 637–643.

Shobert, E.I. (1983). What happens in EDM, In: *Electrical Discharge Machining: Tooling, Methods and applications*, E.C. Jameson (Ed.), 3-4, Society of Manufacturing Engineers, Dearborn, Michigan.

Simao, J.; Lee, H.G.; Aspinwall, D.K.; Dewes R.C. & Aspinwall, E.M. (2003). Workpiece surface modification using electrical discharge machining, *Int. J Mach. Tool. Manu.*, 43, 2, 121-128.

Starke E.A. Jr. & Staley, J.T. (1996). Application of modern aluminum alloys to aircraft, *Progress in Aerospace Sciences*, 32, 2-3, 131-172, ISSN 0376-0421.

Tan, P.C. & Yeo, S. H. (2008). Modelling of overlapping craters in micro-electrical discharge machining, *J Phys. D: Appl. Phys.*, 41, 205302 (12 pp)

Tsai, H.C.; Yan, B.H. & Huang, F.Y. (2003). EDM performance of Cr/ Cu based composite electrodes, *Int. J Mach. Tool. Manu.*, 43, 3, 245–252

Yoshikawa, H. & Nishiyawa, A. (1999). CVD diamond coated inserts for machining high silicon aluminum alloys, *Diamond and RelatedMaterials*, 8, 1527–1530.

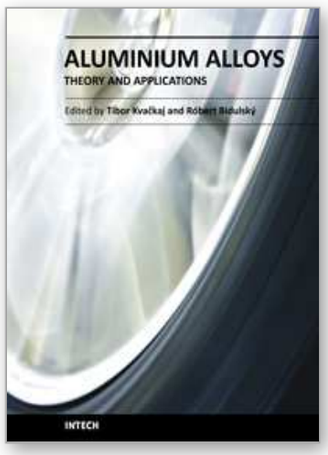


**Aluminium Alloys, Theory and Applications**

Edited by Prof. Tibor Kvackaj

ISBN 978-953-307-244-9
Hard cover, 400 pages
**Publisher** InTech
**Published online** 04, February, 2011
**Published in print edition** February, 2011

The present book enhances in detail the scope and objective of various developmental activities of the aluminium alloys. A lot of research on aluminium alloys has been performed. Currently, the research efforts are connected to the relatively new methods and processes. We hope that people new to the aluminium alloys investigation will find this book to be of assistance for the industry and university fields enabling them to keep up-to-date with the latest developments in aluminium alloys research.

**How to reference**

In order to correctly reference this scholarly work, feel free to copy and paste the following:

Andrea Gatto, Elena Bassoli and Luca Iuliano (2011). Performance Optimization in Machining of Aluminium Alloys for Moulds Production: HSM and EDM, Aluminium Alloys, Theory and Applications, Prof. Tibor Kvackaj (Ed.), ISBN: 978-953-307-244-9, InTech, Available from: http://www.intechopen.com/books/aluminium-alloys-theory-and-applications/performance-optimization-in-machining-of-aluminium-alloys-for-moulds-production-hsm-and-edm

INTECH
open science | open minds

**InTech Europe**
University Campus STeP Ri
Slavka Krautzeka 83/A
51000 Rijeka, Croatia
Phone: +385 (51) 770 447
Fax: +385 (51) 686 166
www.intechopen.com

**InTech China**
Unit 405, Office Block, Hotel Equatorial Shanghai
No.65, Yan An Road (West), Shanghai, 200040, China
中国上海市延安西路65号上海国际贵都大饭店办公楼405单元
Phone: +86-21-62489820
Fax: +86-21-62489821

IntechOpen